buildings

MDPI

Article

Effect of Dynamic Loads on the Long-Term Efficiency of Liner Layers

Ahmed M. Al-Mahbashi and Ahmed Alnuaim *

Department of Civil Engineering, College of Engineering, King Saud University, P.O. Box 800, Riyadh 11421, Saudi Arabia
* Correspondence: alnuaim@ksu.edu.sa

Abstract: The liner layers of natural sand-clay mixtures are extensively used in a range of geotechnical and geoenvironmental projects. In many of these projects, these layers are exposed to dynamic loads or waves due to natural seismic earthquakes or due to human activities, such as machine vibrations, traffic repeated loads, and other impact loads. The permeability of liners is a key property and should be adequately designed to sustain these loads during their lifetime of serviceability. This study sought to evaluate the possible effects of dynamic loads on the efficiency of two different sand-expansive clay (SCL) liners during their lifetime. This was achieved through experimental tests for two series; the first series was subjected to dynamic loads (up to 500 cycles) using the triaxial dynamic system and then tested for permeability for a long period of up to 100 days. The permeability results were compared with the second series tested without being subject to dynamic loads. The dynamic properties for both liners, such as the shear modulus (G), damping ratio (D), and degradation index (δ) were determined and discussed. The results indicated that both materials showed significant degradation with an increase in cycles of dynamic loads; most of the degradation took place during the first 100 cycles. In consequence, the dynamic loads induced a significant effect on the performance of the liners during their lifetime (reducing the permeability by more than six times). These effects were time-dependent and should be taken into account during the design phases.

Keywords: dynamic loads; sand-clay liners; permeability; lifetime; long-run conditions

check for updates

Citation: Al-Mahbashi, A.M.; Alnuaim, A. Effect of Dynamic Loads on the Long-Term Efficiency of Liner Layers. *Buildings* **2023**, *13*, 688. https://doi.org/10.3390/buildings13030688

Academic Editor: Gianfranco De Matteis

Received: 6 February 2023
Revised: 27 February 2023
Accepted: 2 March 2023
Published: 6 March 2023

Copyright: © 2023 by the authors. Licensee MDPI, Basel, Switzerland. This article is an open access article distributed under the terms and conditions of the Creative Commons Attribution (CC BY) license (https://creativecommons.org/licenses/by/4.0/).

1. Introduction

The use of sand-clay liner layers has been widely applied in a range of geotechnical (e.g., protection of road and slope shoulders, dams, foundations for offshore machines, etc.) and geoenvironmental projects (e.g., hydraulic barriers, buffers for waste disposals, etc.) due to their low-cost and environmentally friendly properties.

Dynamic loads or waves can be generated directly due to natural seismic earthquakes or as a response to different activities, such as machine vibrations, oceanic or sea waves, heavy and fast traffic loading in transportation systems (i.e., land, water, or air), and other impact loads. In such circumstances, dynamic properties, such as the shear wave velocity, shear modulus, and stiffness degradation, require analysis when designing engineering projects subject to dynamic loads [1]. To assess earthquake ground motion response, the required parameters, such as the frequency energy, amplitude, pulse, etc. have recently been identified and modeled to satisfy the requirements of seismic structural analysis [2,3]. The liner layers can be exposed to dynamic loads during their serviceability or construction phases (e.g., the vibration of construction machines and impact loads). The effect of these dynamic loads on the performance of liners during their lifetime should be addressed for adequate and sustainable design.

The dynamic properties of fine- and coarse-grained soils have been studied by several researchers using resonant column or dynamic triaxial tests (i.e., [4–9]), with the results indicating variation in material degradation as a response to these loads. Recently, Pandya

and Sachan [9] investigated the dynamic properties of compacted cohesive soils under different frequency, amplitude, and consolidation conditions. The results indicated that the magnitude of stiffness degradation increased with increase in amplitude. The shear modulus and damping ratio also increased by increasing the frequency of loading. Other studies have reported that the strength (cohesion and internal friction angle) of treated expansive soil specimens tested under saturated conditions show a reduction with increase in the cycle number (e.g., Wang et al. [5]).

Methods proposed for measuring the shear wave velocity in the laboratory have also been developed using split sensor techniques adapted to oedometer or triaxial systems. The bender element method (BE) has been effectively used worldwide. The method has been adopted in the past [10,11], and has recently been simplified to enable its use at low cost. The two pairs of bender elements (i.e., probes) were adapted to the testing systems (i.e., triaxial or odometer) and inserted into the ends of the soil specimen; a sinusoidal wave is generated from the first element and received by the second element on the other end depending on the travel distance in the body of the soil specimen between the pair of BEs.

The hydraulic conductivity of liner layers is a factor in adequate and sustainable design. Studies conducted by Al-Mahbashi et al. [12,13]) examined the sustainability and efficiency of liner layers during the long run of their lifetime. The results indicated degradation in hydraulic conductivity with time due to the migration of fine content. Abdolahzadeh et al. [14] observed a reduction in flow rate through a cover layer of sand and gravel during long-run performance. Al-Mahbashi and Dafalla [15] showed that the application of a surcharge load of 30 kPa to sand-expansive clay liners reduced the flocculation of the permeability values and provided a more stable trend over the long run. In addition, Alnuaim et al. [16] reported an increase in stability for sand-expansive clay liners using crushed limestone powder.

Studies that address the dynamic properties of liners susceptible to dynamic loading are rare in the literature. Pan et al. [17] evaluated the dynamic properties of different mixtures of sawdust with sand using dynamic triaxial tests. The results indicated a reduction in the shear modulus and damping ratio with increase in sawdust materials. Furthermore, there have been few studies that have examined the hydraulic conductivity of liner layers that are exposed to dynamic loading. Sun et al. [18] examined the effects of cyclic loading on the permeability of soft clay. The results indicated significant changes in permeability. The study was carried out over a short period (a matter of hours) and there was no evaluation of the permeability when subject to a cyclic loading for a longer duration. In addition, there are no available studies that have evaluated the efficiency of liners over the long run of their lifetime when subject to dynamic loads. The purpose of this study was to examine the long-term efficiency of liners subjected to dynamic loads. The specimens were initially subjected to cyclic dynamic loads using the triaxial system for about 500 cycles, and the dynamic properties of the tested specimens were identified. The shear wave velocity was measured using the bender elements test (BE). The data obtained from cyclic dynamic loading were analyzed and the shear modulus, damping ratio, and degree of stiffness degradation were calculated. After dynamic loading, the specimens were tested to determine the long-term permeability (up to 100 days). The results were compared to identical specimens not subjected to dynamic loading to evaluate the possible effects of dynamic loads on the lifetime of liner layers.

2. Materials and Methods

The liner materials used in this study utilized two mixtures of sand with expansive clay. The first mixture consisted of 30% clay, hereinafter referred to as sand clay liner 30 (SCL30); the second consisted of 20% clay (SCL20). The sand was a local material obtained from the vicinity of Riyadh city; the specific gravity for this sand was estimated at 2.67 (ASTM D854 [19]). The particle size distribution curve of this sand was determined in the laboratory using a sieve analysis test following the requirements of ASTM D6913 [20] and is shown in Figure 1. The data on this curve indicated that the uniformity coefficient (C_u) was

1.745, and the coefficient of concavity (C_c) was 0.945. Based on these values (C_u and C_c), and according to the classification system ASTM D2487 [21], the sand was classified as poorly graded sand.

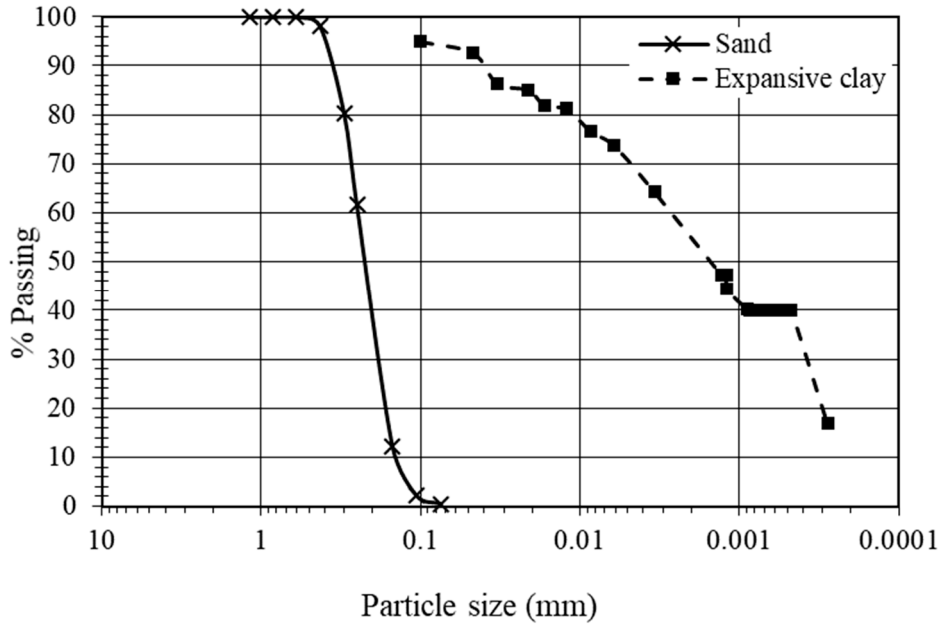


Figure 1. Particle size distribution for sand and expansive clay.

The expansive clay used in this study was obtained from the eastern region of Saudi Arabia, specifically from Al-Qatif city. The characterization of this clay was conducted in the laboratory and revealed that the liquid limit, plastic limit, and shrinkage limit were 160%, 60%, and 13%, respectively (as per ASTM D4318 [22]). The specific gravity of this clay was 2.71 (ASTM D854 [19]), and, according to the unified classification system, was defined as a high-plasticity clay (ASTM D2487 [21]). The particle size distribution curve was obtained from the sedimentation test using a hydrometer analysis test (ASTM D7928 [23]) and is presented in Figure 1. The mineralogical analysis, conducted using XRD, indicated that the clay consisted of a considerable amount of montmorillonite [24]; this amount was estimated to be up to 23% [25]. As a result of the abundance of this mineral, the clay had a high swell potential of between 16 to 18% and a swelling pressure of about 550 kPa [26–28].

3. Specimen Preparation

The mixtures of dry sand and expansive clay were thoroughly mixed with different moisture contents and stored overnight to achieve homogeneity. Then, a series of standard compaction tests were performed to determine the compaction curves following ASTM D698 [29]. The maximum dry density and optimum moisture content for both mixtures, SCL30 and SCL20, obtained from compaction curves were 18.03 kN/m^3, 13.70%, and 18.29 kN/m^3, 13.60%, respectively. The specimens were prepared with optimum moisture content and then statically compacted in layers (i.e., 50 mm diameter and 100 mm high) to achieve maximum dry density using a plunger mold as per BS EN 13286-53 [30]. Special grooves of about 1.5 mm depth were prepared on the top and bottom sides of the compacted specimen using a predesigned pattern (Figure 2a). These grooves were used later to host and fix the bender elements (Figure 2b) at the top and bottom of the soil specimen while conducting a shear wave velocity test.

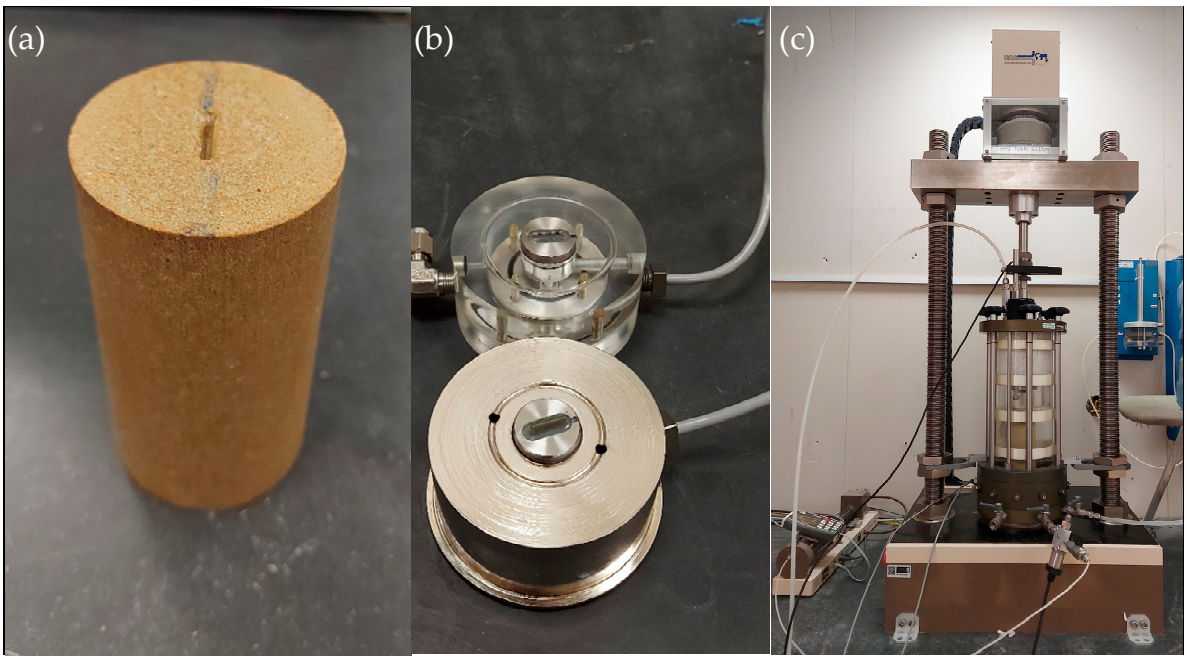


Figure 2. (**a**) Prepared specimen for dynamic loading test, (**b**) bender elements, and (**c**) dynamic triaxial system.

4. Testing Procedures

In this study, the specimens of different liners were subjected to cyclic dynamic loads using a dynamic triaxial apparatus; then, the specimens were tested for permeability for long periods (around 100 days). The following sections describe in detail the experimental work undertaken for these tests.

4.1. Dynamic Loading Test

This section is divided into subheadings. It provides a concise and precise description of the experimental results, their interpretation, as well as the conclusions that can be drawn.

A cyclic dynamic loading test was performed on saturated specimens for both liner mixtures (SCL30 and SCL20) using a dynamic triaxial system (Figure 2c) under stress control conditions. The test included a saturation stage, consolidation stage, and then dynamic loading. A bender element test was conducted after the consolidation stage to measure the shear wave velocity of the tested soils. The dynamic triaxial system consisted of a pressure cell, a dynamic actuator load unit, and pressure control units. To begin with, the compacted specimen was fixed on the central pedestal of the pressure cell. Two attached bender element (BL) probes were provided and installed on special grooves (of 1.5 mm depth) prepared at the ends of the tested specimen during compaction (Figure 2a,b). The grooves were coated with a thin layer of silicon grease to ensure good insulation and waterproofing. These elements represented the wave transmitter (installed on the bottom of the tested specimen) and the wave receiver (installed on the top of the specimen). The setup of the specimen and bender element probes were encased by membrane rubber. The rubber rings enabled tightening of the membrane with the base pedestal and the attached top cap to prevent water leakage.

The specimen was then ready to commence the saturation process. An initial back pressure of 20 kPa was gradually applied concurrently with imposing a cell pressure of 30 kPa to conduct the first flushing. This process was necessary to expel the air from the surroundings of the specimen and the large pores. After this process (flushing), a forced saturation process was applied through successive stages or increments of back pressure (i.e., 40 kPa increments). Each stage was maintained until the monitored volume of pore water was dissipated and then the B-value was checked. The process was continued until a

B value of more than 96% was achieved. This condition was achieved after about ten stages (i.e., at a back pressure of 450 kPa). When the saturation stage was completed, the isotropic consolidation was started by applying a cell pressure at a rate of 8 kPa per hour up to an effective consolidation stress of 100 kPa. The change in volume versus time was monitored and consolidation was confirmed when there was no further change in the curve for the last 24 h; the consolidation stage took from 6 to 20 days.

The dynamic load stage was conducted by applying a cyclic dynamic load for 500 cycles. The selected cyclic stress ratio was 0.35 and the amplitude of cyclic stress was 0.14 for the test. The frequency during dynamic testing was 1 Hz to stimulate the majority of expected dynamic loads.

4.2. Shear Wave Velocity

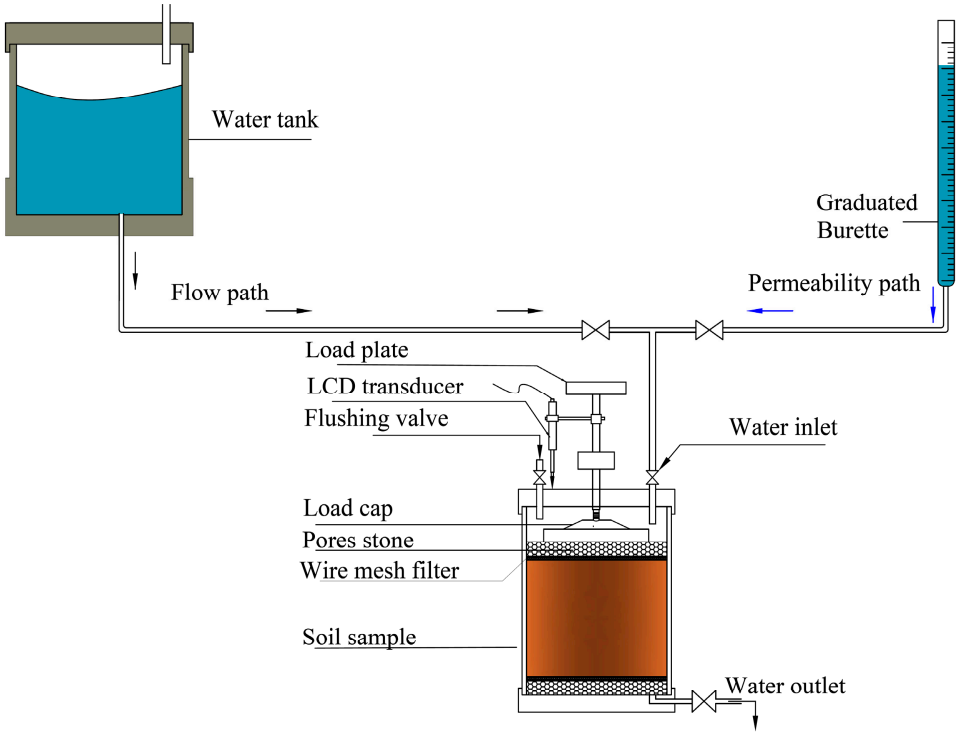
The bender element tests were conducted after the isotropic consolidation stage to measure the shear wave velocity. The set of bender elements at the top and bottom of the soil specimen (Figure 2b) was adopted for this purpose. The sine-wave form was selected and generated from the bottom of the specimen at different levels of frequency (i.e., from 4000 to 10,000 Hz). This wave was propagated through the clear length of the specimen measured tip-to-tip (L_{tt}) and received on the other end. Sine-wave pulses have been proven to produce a more reliable measurement of arrival time rather than square-wave pulses [31]. The different types of waves and their application were summarized by Da Fonseca et al. [32]. Ogino et al. [33] conducted a series of bender element tests on specimens of different sands and clayey soils to measure the shear wave velocity through these soils. The measurements were performed considering three different techniques, namely: the time domain, cross-correlation, and the frequency domain. It could be inferred from this study that the time domain technique using beak-to-beak measured the shear wave velocity effectively. Furthermore, even with this technique, there is no reliable direct measurement of travel time [34]. In this study, the relationship between wavelengths (n = F**t*) and frequency (F) following the π-method was used for calculating the shear wave velocity [32,34].

4.3. Long-Term Permeability

After conducting dynamic cyclic loading, the specimens were carefully trimmed to create a permeability cell about 30 mm high. Figure 3a shows the specimen inside the extruder mold with the set of filters including pore stones, wire mesh, and the perforated plate applied at the top and bottom of the specimen. The setup was prepared on the testing cell (Figure 3a) and the falling head permeability test was performed following ASTM D5856 [35]. The setup consisted of a permeability cell, water tank, and graduate burette, as shown in Figure 3b. The water tank supplied water to the top of the specimen during flow or discharge, and the additional valve was used to transfer the system to permeability measurement through a graduated burette (Figure 3b). The measurement of permeability was started when steady flow has achieved; this could be judged when the average of subsequent measurements (i.e., four times) fell within $\pm$25% of the mean value. The first measurements of permeability were recorded; then, the specimen was subjected to continuous flow. During the period of continuous flow, the permeability was measured several times per day (i.e., up to three times).



(**a**)



(**b**)

Figure 3. (**a**) Specimen with cell setup, and (**b**) sketch of the permeability test.

5. Results and Discussion

5.1. Stress-Strain Behavior during Dynamic Cyclic Loading

Stress-strain behavior for liner materials is a key factor for modeling and accurate design purposes. This behavior was described in this section under the effect of applied dynamic loads (i.e., up to 500 cycles). Figure 4a,b show the stress-strain relation during different sinusoidal cyclic loading (i.e., 1, 8, 100, and 500) for both soils; the nonlinear behavior induced a hysteric loop—the area of this loop is referred to as the hysteric loop. It is clear from the figures that the hysteric loop was non-concentric, asymmetric, and varied

with the number of cyclic loadings. The area of this loop was increased with increase in the cycle number up to a certain level for both soils. The shapes of the hysteric loops were close to each other; the tips of the loops were closed to a slightly rounded pointed form. This was due to the higher content of sand rather than clay for both soils of 80 and 70%. The earliest studies conducted on soils regarding their response to dynamic loads [36,37] indicated that the tips of the hysteresis loop are pointed for clean sand and tend to be rounded for clays. By the same analogy, the nonlinearity of stress-strain behavior is greater for sandy soils than clayey soils. The soil with the higher clay percentage, SCL30 (Figure 4b), showed a higher creep response on the skeleton under dynamic loading compared to the SCL20 specimen (Figure 4a). This was attributed to the higher viscosity [38,39].

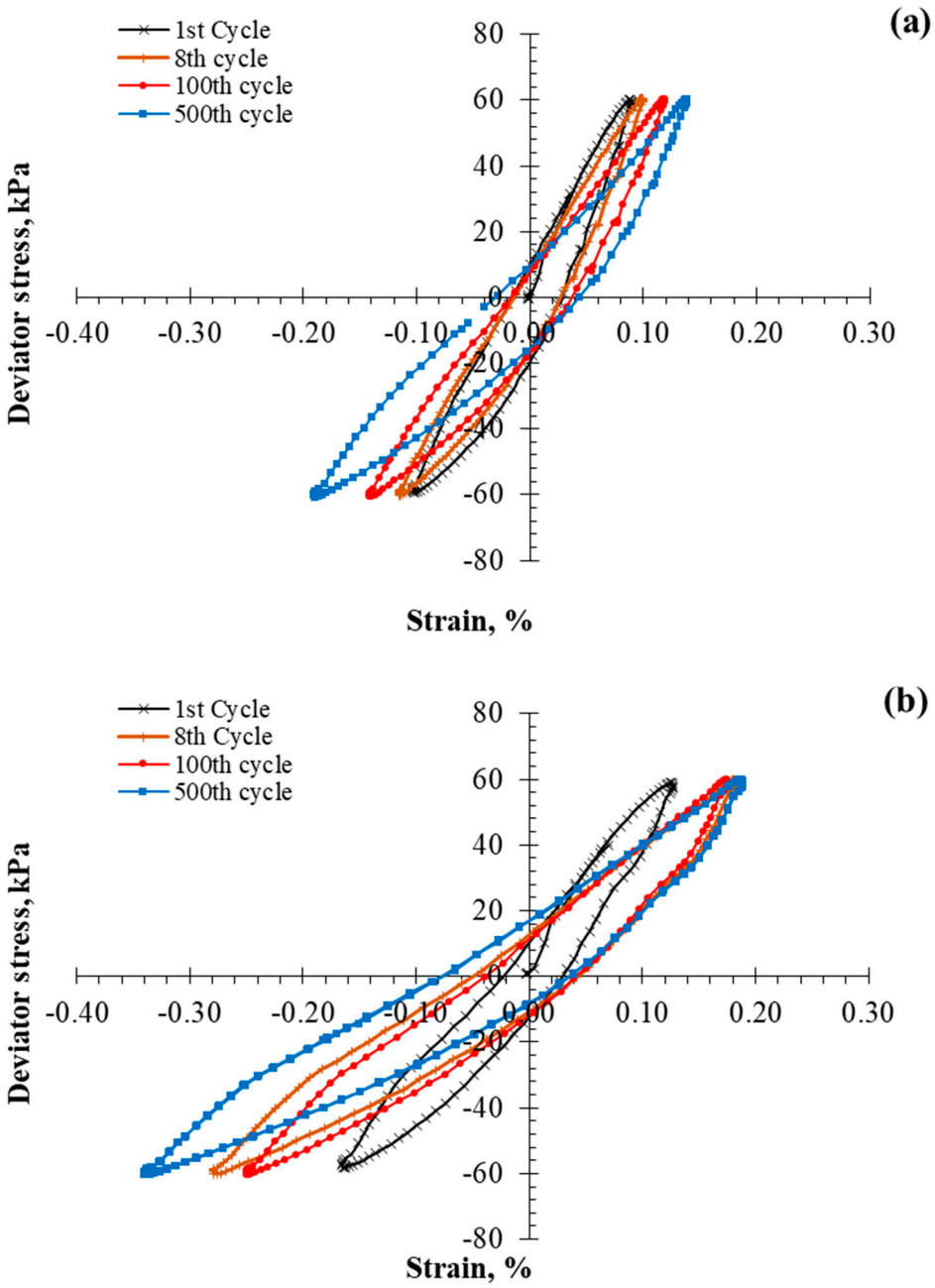


Figure 4. Stress-strain hysteric loop during dynamic loading at selected cycles for (**a**) SCL20 and (**b**) SCL30.

5.2. Damping Ratio

The phenomena of damping of materials during dynamic loading can be defined as a measure of energy dissipation during soil response to this load. In this study, the damping ratio was calculated at different loading cycles (i.e., 1, 3, 8, 10, 100, 200, 300, 400, and 500), taking into account the asymmetric analogy of the hysteric stress-strain loop. Previous studies have reported that under asymmetric conditions of the hysteric loop, higher damping ratio values (i.e., up to 40 to 70%) are obtained than the values obtained under symmetric conditions [40,41]. Figure 5 shows the typical shape of the hysteresis loop. The calculation method was conducted following ASTM D3999 [42], as shown in Equation (1).

$$D_{\%} = \frac{A_L}{4\pi A_T} \times 100 \quad (1)$$

where A_L is the area of the entire hysteresis loop and A_T is the area of a shaded triangle (Figure 5).

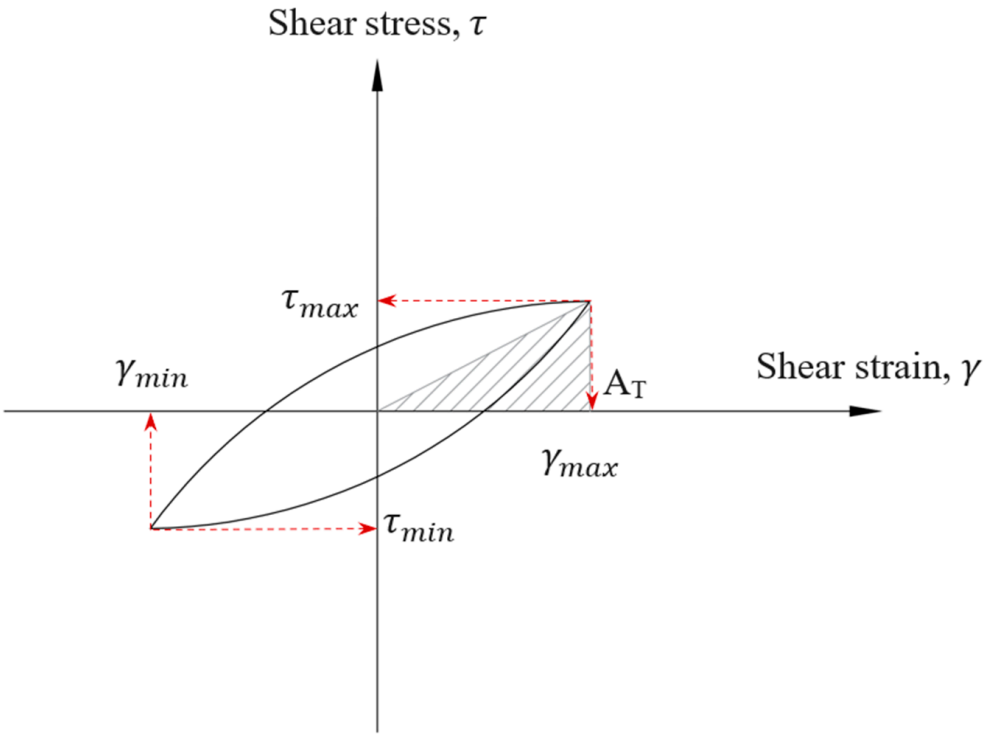


Figure 5. Typical hysteresis loop during dynamic loading.

Figure 6 shows the calculated values of the damping ratio for both soils; the values tended to increase as the loading cycles increased. The damping effect exhibited in soils under dynamic loads has been attributed to the mechanisms of hysteric damping, the viscosity of soil (i.e., skeleton creep), and the viscosity of pore fluids [5,37,38]. Soil type, level of shear strain, and frequency are the most important factors that control soil damping (e.g., Presti et al. [39]). It is worth noting that the soil with a higher clay or fines portion showed high values of damping and the difference was increased with increase in the loading cycles. Lanzo and Vucetic [37] showed that the damping ratio increased about three times with increase in soil plasticity (PI) up to 60%. It was also found that the damping of soils with low plasticity was more sensitive to cyclic loading and confining pressure.

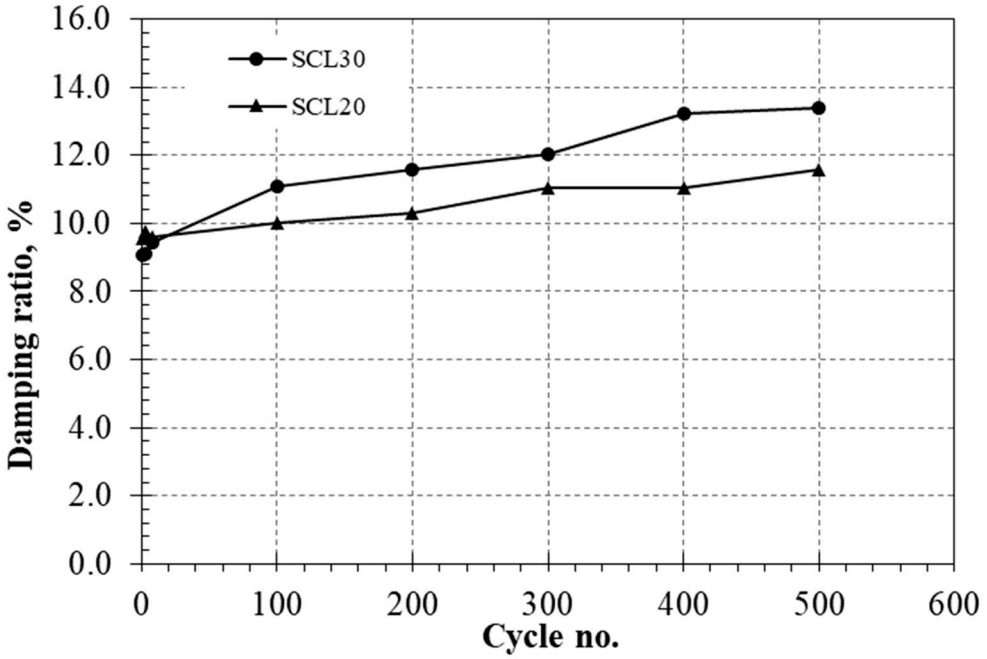


Figure 6. Damping ratio versus dynamic load cycles.

5.3. Shear Modulus (G) and Degradation Index (δ) Ratio

In this study, the shear modulus during dynamic loading was calculated based on the typical pattern of a stress-strain hysteric loop (i.e., Figure 5). The secant shear modulus was calculated for each cycle of dynamic loading and is illustrated in Figure 7 for both soils. The results showed significant degradation in the shear modulus (i.e., around 40% reduction) with increase in dynamic load cycles up to 500 cycles. The sharp slope at the first tenth cycle indicated high degradation at this level of cycles, similar to the behavior reported in several previous studies (e.g., [41]). The major part of degradation, of around 80%, took place during the first 100 cycles. It is worth noting that the shear modulus of soil with a higher fine percentage (SCL30) showed lower values than the other soil. This finding is inconsistent with those of studies that reported a significant reduction in shear modulus with increase in the fine percentage of granular materials (e.g., [6,43]).

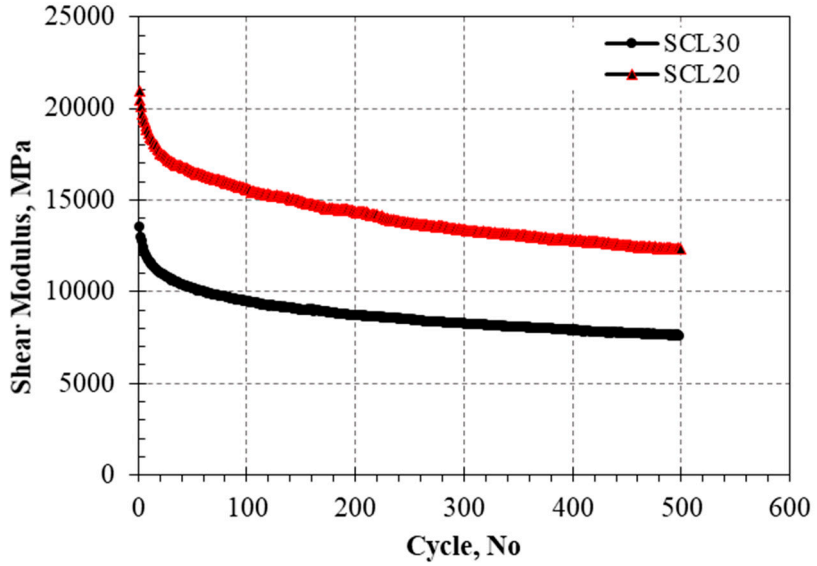


Figure 7. Shear modulus versus cycles of dynamic loading.

The high values of the damping ratio (i.e., Figure 6) indicate material degradation. In this study, the degradation index (δ) for the materials used was represented in terms of the shear modulus (G/G_0). The shear modulus of the first cycle of dynamic loading (G_0) was considered in this calculation. Figure 8 shows the degradation index, along with the cycles of dynamic loading up to 500 cycles. Both materials showed a considerable degradation index of more than 0.6. The SCL30 specimen exhibited a small increase in degradation index compared to SCL20. This can be attributed to the higher percentage of clay, more fines may have enabled the formation of more clay bridges between particles, and this microfabric affecting the clay–sand interaction [44].

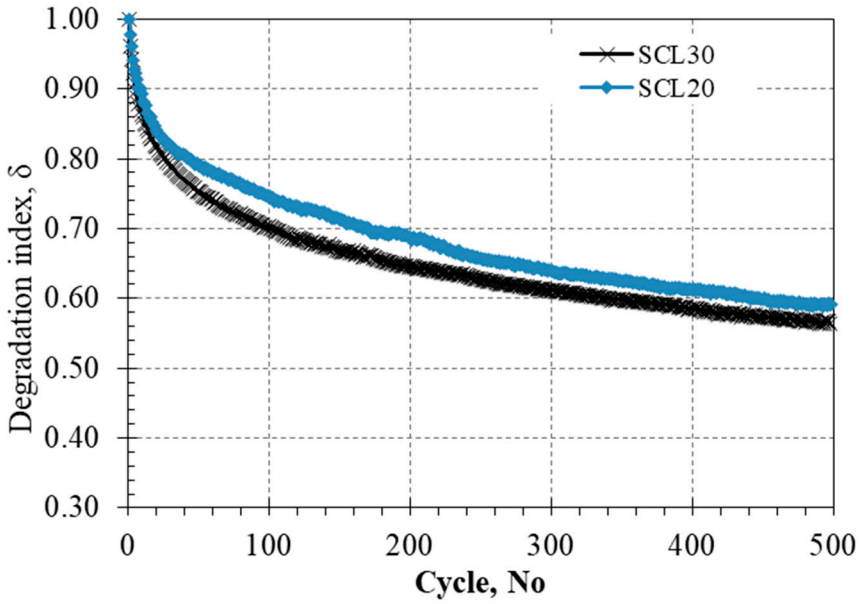
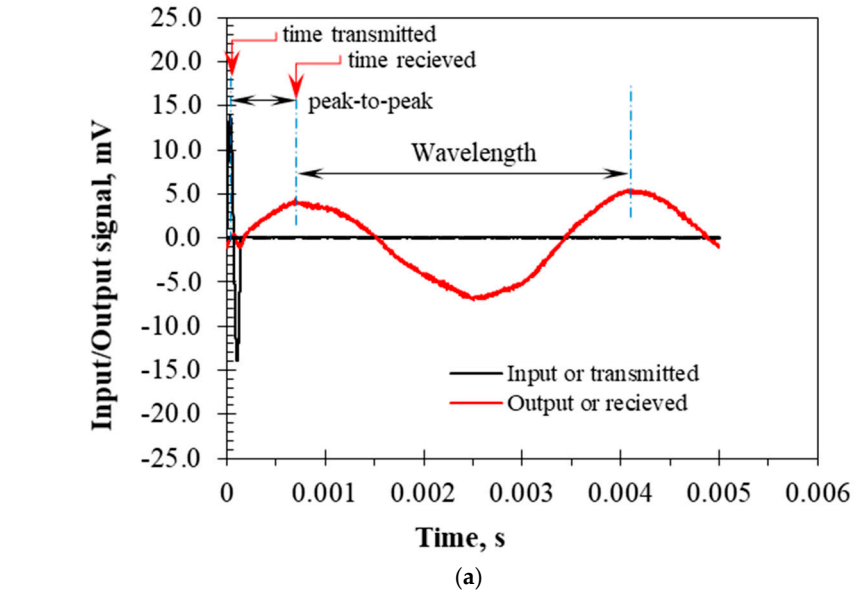


Figure 8. Degradation index versus dynamic load cycles.

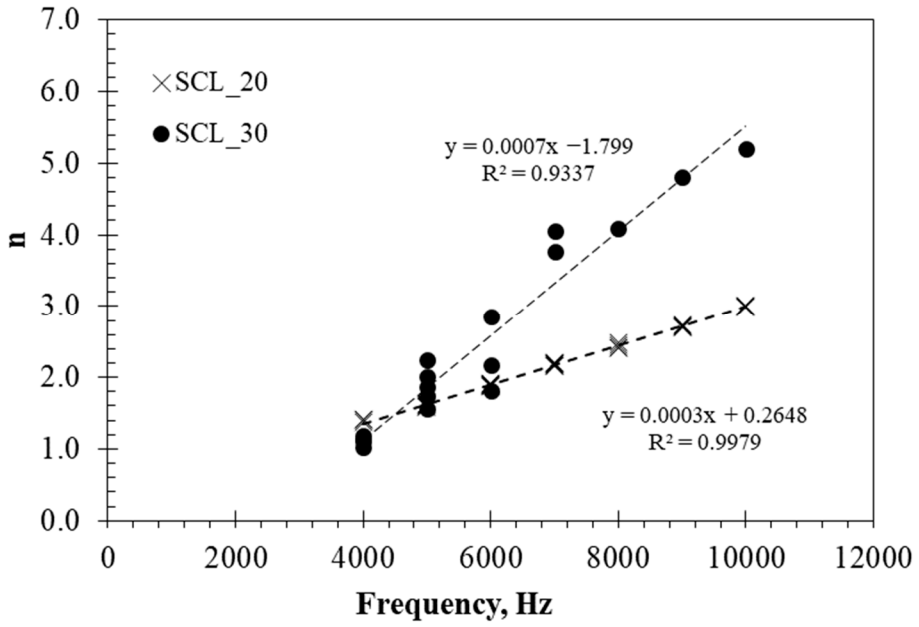
5.4. Shear Wave Velocity

Several attempts were made to obtain the shear wave velocity at different frequencies between 4 and 10 kHz. The signals received were analyzed to obtain the firm shape. An example of one attempt for the generated and received waves at a frequency of 7000 Hz is shown in Figure 9a. The times for the generated and received waves with wavelength are illustrated in the same figure. The peak-to-peak distance between the transmitter and the first generated wave (Figure 9a) was used to estimate the arrival time. The relationship between the wavelengths (n = f*Δt) and frequency following the π-method performed for SCL20_Dy is shown in Figure 9b. This method has been described in [32,34] and compared with different methods in [45]; the slope of the best-fit line represents the arrival time (t). The clear length of the specimen calculated from tip to tip (L_{tt}) was utilized to compute the shear wave velocity (Vs) following Equation (2). The results obtained by this method showed values for the shear wave velocity of 247 and 155 m/s for SCL20 and SCL30, respectively. It is of note that the shear wave velocity on sand was higher than for the clayey soil and that the fine percent with void ratio played a key role in the propagation of shear waves [46], and these are govern the obtained values in this study.

$$V_s = \frac{L_{tt}}{t} \quad (2)$$



(**a**)



(**b**)

Figure 9. (**a**) Example of generated and received waves versus time, and (**b**) wavelength versus frequency for tested liners.

5.5. Long-Term Permeability

This section highlights the effect of dynamic loads on the long-term permeability (around 100 days) for different liner specimens (SCL30_Dy and SCL20_Dy). As stated in the previous sections, continuous flow was applied during the entire period. The obtained results were compared with identical specimens of both liners that were examined under similar conditions without applying dynamic loads (SCL30 and SCL20). Figure 10 shows the variation in permeability with time for SCL30 before and after exposure to dynamic cyclic loads (SCL30_Dy). It is clear that the dynamic load had a significant influence on the permeability up to a certain period of time (i.e., nearly 80 days).

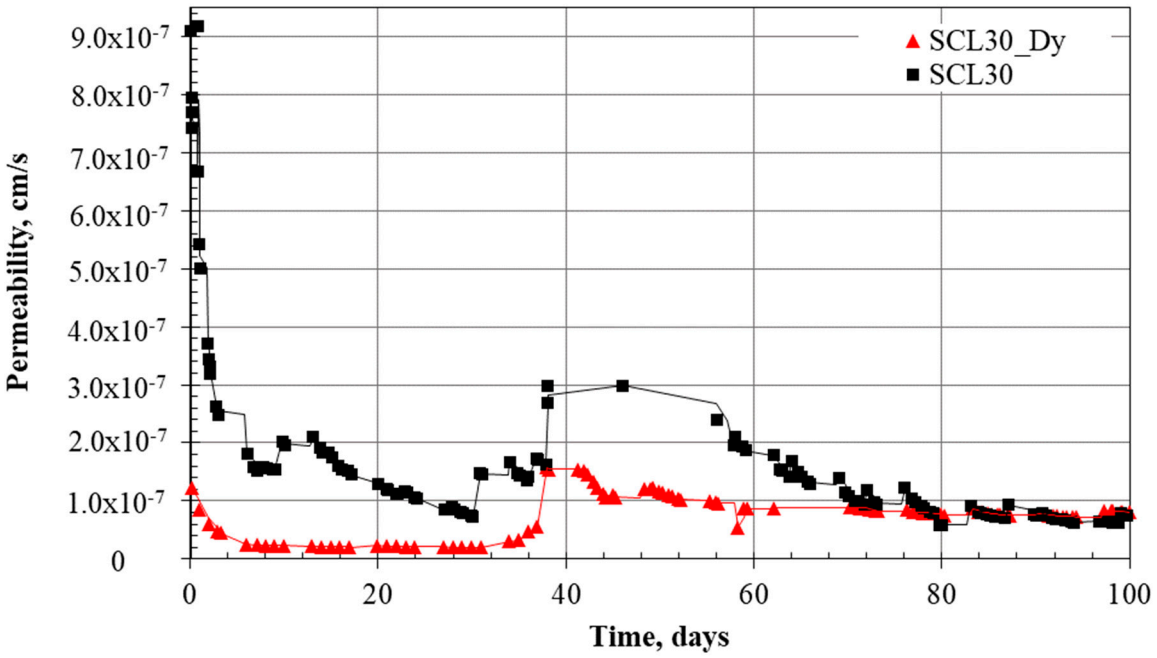


Figure 10. Variation in permeability with time under continuous flow for SCL30 specimens.

At the initial stage of the test (before applying continuous flow), the permeability of the specimen subjected to dynamic loads (SCL30_Dy) was reduced by more than six times. This was attributed to the degradation taking place in the internal structure of the specimen due to dynamic load turn, which partially blocked pores and reduced the void ratio which governed the permeability [47–49].

As the continuous flow continued to advance, a drop in permeability was detected during the first week. The drop in the permeability values for specimen SCL30 was around six times, while the specimen subjected to dynamic loads (SCL30_Dy) showed more stability with a small drop in the permeability values. This drop in permeability was mainly attributed to the collapse of the inner structure (large pores), with similar behavior being reported in several previous studies [15,50,51]. Specimen SCL30_Dy was densified due to the dynamic loads and the collapse of the inner structure was minimal. With continuous flow maintained through the specimen, the fine materials started to migrate, and the permeability periodically increased showing repeated peaks at 10 and 40 days. On the other hand, for SCL30_Dy, the permeability values showed a more stable trend except for a small peak at 40 days. Al-Mahbashi et al. [12] measured the fine percent before and after applying continuous flow for long periods. A notable reduction in fine percent was observed varying from 7 to 15% due to the migration of fines with the flow. Similar behavior was previously reported by Sharma and Yortsos [52]; this reduction was also dependent on the type and content of fines for each mixture. The process of migration of fines and the collapse of structure was repeated for a long period until stable conditions were achieved; this behavior was reported by Al-Mahbashi and Dafalla [15] for a sand and bentonite mixture. In this study, the permeability values for both specimens of SCL30 and SCL30_Dy converged and exhibited similar behavior after approximately 80 days with a stable trend. Similar behavior was observed for the SCL20 specimens, as shown in Figure 11; this mixture showed higher permeability values. The peak or rise of permeability in the earliest stage (i.e., around 10 days) for specimen SCL20 before applying dynamic loads was attributed to a similar reason, previously mentioned, of fine migration during flow conditions. The changes in permeability were more than those for SCL30, and stable conditions were achieved faster at around 30 days. The overall evaluation of results revealed that consideration of suspected dynamic loads when designing the mixtures of the liner layers was valuable for accurate and sustainable performance.

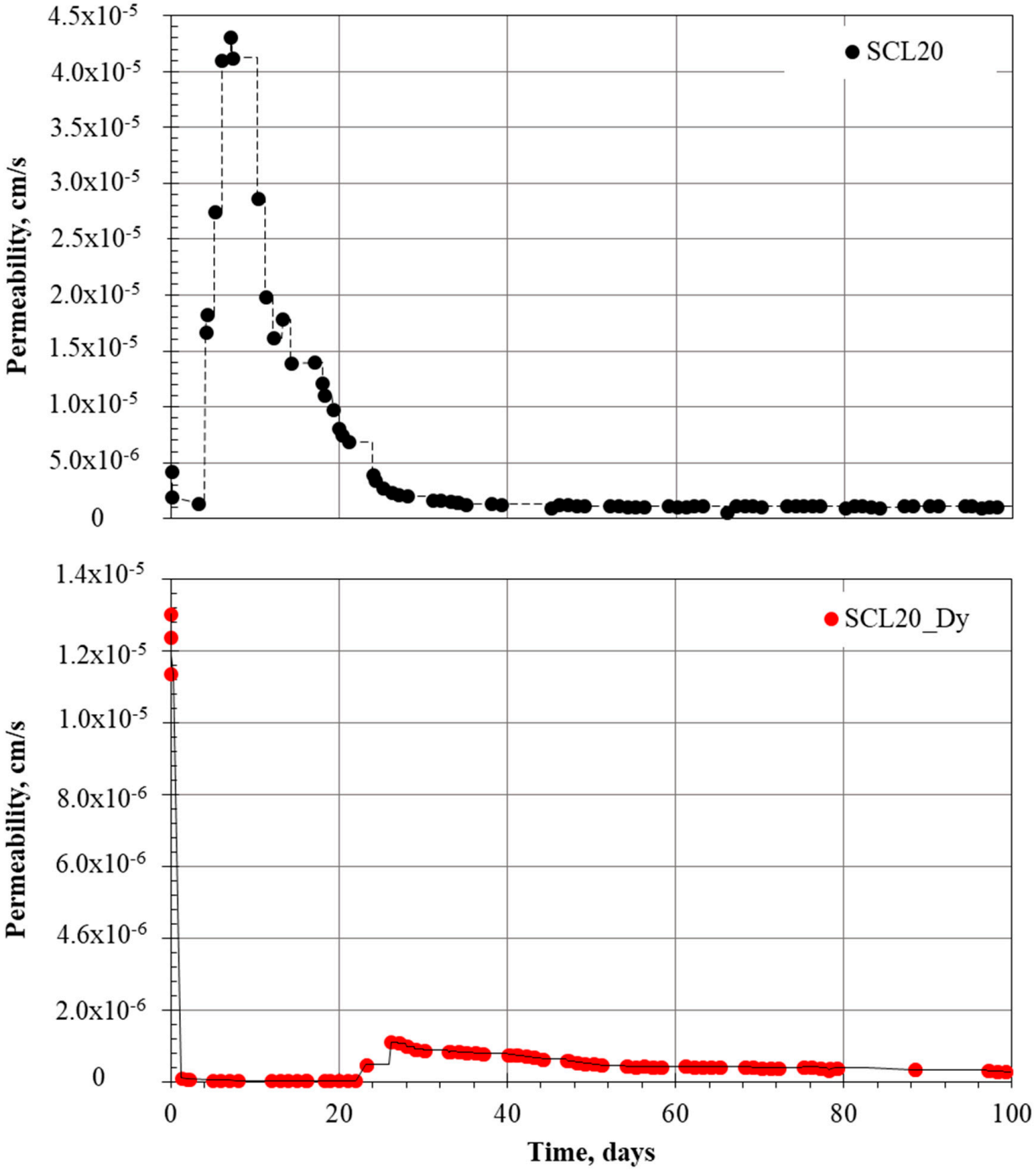


Figure 11. Variation in permeability with time under continuous flow for SCL20 specimens.

6. Summary and Conclusions

The testing program conducted in this study has provided some insights into the effect of dynamic loads on the long-term efficiency of liner layers. The following conclusions can be drawn:

- The nonlinear behavior of stress-strain induced a non-concentric, asymmetric hysteric loop deformation of loop shape with cycles of loading indicating structural creep, especially for the soil with a higher fine percent, SCL30.
- The damping ratio measured for specimens subjected to dynamic loads reached 12% and 14% for SCL20 and SCL30, respectively. The degradation factor indicated that the majority of deterioration took place during the first 100 cycles.

- The shear modulus of specimens with low fine percent was higher by about 50%, and both specimens lost around 30% from their shear modulus due to dynamic loads.
- The specimens subjected to dynamic loads showed a significant drop in permeability values in the early stages (before applying continuous flow).
- During the continuous flow, the specimens subjected to dynamic loads showed less variation in permeability and a stable trend with time due to structure densification.
- The permeability is a key factor when designing liner layers for different geotechnical and geoenvironmental projects. Consideration of the possible effects of dynamic loads is highly recommended for sustainable and adequate performance during their lifetime.

Author Contributions: Conceptualization, A.M.A.-M. and A.A.; methodology, A.M.A.-M.; software, A.M.A.-M.; validation, A.M.A.-M.; formal analysis, A.M.A.-M.; investigation, A.M.A.-M.; resources, A.M.A.-M. and A.A.; data curation, A.M.A.-M.; writing—original draft preparation, A.M.A.-M.; writing—review and editing, A.M.A.-M. and A.A.; visualization, A.M.A.-M.; supervision, A.A.; project administration, A.M.A.-M. and A.A.; funding acquisition, A.A. All authors have read and agreed to the published version of the manuscript.

Funding: Researchers Supporting Project number (RSP2023R285), King Saud University, Riyadh, Saudi Arabia.

Data Availability Statement: The data used to support the findings of this study are included in the figures shown.

Acknowledgments: The authors would like to acknowledge the Researchers Supporting Project number (RSP2023R285), King Saud University, Riyadh, Saudi Arabia.

Conflicts of Interest: The author declares that he has no conflict of interest.

References

1. Luna, R.; Jadi, H. Determination of dynamic soil properties using geophysical methods. In Proceedings of the First International Conference on the Application of Geophysical and NDT Methodologies to Transportation Facilities and Infrastructure, St. Louis, MO, USA, 11–15 December 2000; pp. 1–15.
2. Chen, G.; Yang, J.; Liu, Y.; Kitahara, T.; Beer, M. An energy-frequency parameter for earthquake ground mo-tion intensity measure. *Earthq. Eng. Struct. Dyn.* **2023**, *52*, 271–284. [CrossRef]
3. Chen, G.; Beer, M.; Liu, Y. Modeling response spectrum compatible pulse-like ground motion. *Mech. Syst. Signal Process.* **2022**, *177*, 109177. [CrossRef]
4. Sitharam, T.G.; Govindaraju, L.; Murthy, B.S. Evaluation of liquefaction potential and dynamic properties of silty sand using cyclic triaxial testing. *Geotech. Test. J.* **2004**, *27*, 423–429.
5. Wang, M.; Kong, L.; Zhao, C.; Zang, M. Dynamic characteristics of lime-treated expansive soil under cyclic loading. *J. Rock Mech. Geotech. Eng.* **2012**, *4*, 352–359. [CrossRef]
6. Wichtmann, T.; Hernández, M.N.; Triantafyllidis, T. On the influence of a non-cohesive fines content on small strain stiffness, modulus degradation and damping of quartz sand. *Soil Dyn. Earthq. Eng.* **2015**, *69*, 103–114. [CrossRef]
7. Dammala, P.K.; Kumar, S.S.; Krishna, A.M.; Bhattacharya, S. Dynamic soil properties and liquefaction potential of northeast Indian soil for non-linear effective stress analysis. *Bull. Earthq. Eng.* **2019**, *17*, 2899–2933. [CrossRef]
8. Zhao, F.; Chang, L.; Zhang, W. Experimental investigation of dynamic shear modulus and damping ratio of Qinghai-Tibet frozen silt under multi-stage cyclic loading. *Cold Reg. Sci. Technol.* **2020**, *170*, 102938. [CrossRef]
9. Pandya, S.; Sachan, A. Effect of frequency and amplitude on dynamic behaviour, stiffness degradation and energy dissipation of saturated cohesive soil. *Geomech. Geoengin.* **2022**, *17*, 30–44. [CrossRef]
10. Shirley, D.J.; Hampton, L.D. Shear-wave measurements in laboratory sediments. *J. Acoust. Soc. Am.* **1978**, *63*, 607–613. [CrossRef]
11. Dyvik, R.; Madshus, C. Lab Measurements of Gmax Using Bender Elements. In Proceedings of the Proceedings ASCE Annual Convention: Advances in the Art of Testing Soils Under Cyclic Conditions, Detroit, MI, USA, 24 October 1985; pp. 186–197.
12. Al-Mahbashi, A.M.; Dafalla, M.; Shaker, A.; Al-Shamrani, M.A. Sustainable and Stable Clay Sand Liners over Time. *Sustainability* **2021**, *13*, 7840. [CrossRef]
13. Al-Mahbashi, A.M.; Dafalla, M.; Al-Shamrani, M. Long-Term Performance of Liners Subjected to Freeze-Thaw Cycles. *Water* **2022**, *14*, 3218. [CrossRef]
14. Abdolahzadeh, A.M.; Vachon, B.L.; Cabral, A.R. Assessment of the design of an experimental cover with capillary barrier effect using 4 years of field data. *Geotech. Geol. Eng.* **2011**, *29*, 783–802. [CrossRef]
15. Al-Mahbashi, A.M.; Dafalla, M. Impact of placement and field conditions on hydraulic conductivity and lifetime of liners. *J. King Saud Univ.-Sci.* **2021**, *33*, 101410. [CrossRef]

16. Alnuaim, A.; Dafalla, M.; Al-Mahbashi, A. Enhancement of Clay–Sand Liners Using Crushed Limestone Powder for Better Fluid Control. *Arab. J. Sci. Eng.* **2020**, *45*, 367–380. [CrossRef]
17. Pan, D.; Li, X.; Lu, P.; Chen, Q. Dynamic properties of sand-sawdust mixture for modeling deposit soil. *Appl. Sci.* **2019**, *9*, 3863. [CrossRef]
18. Sun, M.; Yu, J.; Ding, Z.; He, S. Numerical Model about the Influence of Cyclic Load on the Hydraulic Conductivity of Soft Clay. *KSCE J. Civ. Eng.* **2021**, *25*, 4159–4172. [CrossRef]
19. *ASTM D854-14*; Standard Test Methods for Specific Gravity of Soil Solids by Water Pycnometer. ASTM International: West Conshohocken, PA, USA, 2014.
20. *ASTM D6913−04*; Standard Test Methods for Particle-Size Distribution (Gradation) of Soils Using Sieve Analysis. ASTM Standard International: West Conshohocken, PA, USA, 2009.
21. *ASTM D2487-17*; Standard Practice for Classification of Soils for Engineering Purposes (Unified Soil Classification System). ASTM International: West Conshohocken, PA, USA, 2017. [CrossRef]
22. *ASTM D4318*; Standard Test Methods for Liquid Limit, Plastic Limit, and Plasticity Index of Soils. ASTM: West Conshohocken, PA, USA, 2017.
23. *ASTM D7928-17*; Standard Test Method for Particle-Size Distribution (Gradation) of Fine-Grained Soils Using the Sedimentation (Hydrometer) Analysis. ASTM International: West Conshohocken, PA, USA, 2017.
24. Al-Mahbashi, A.M.; Al-Shamrani, M. Long-term and immediate effects of freeze–thaw cycles on the resilient modulus of treated expansive subgrades. *Road Mater. Pavement Des.* **2022**, 1–14. [CrossRef]
25. Rafi, A. Engineering Properties and Mineralogical Composition of Expansive Clays in Al-Qatif Area. Ph.D. Thesis, King Fahd University of Petroleum and Minerals (KFUPM), Dhahran, Saudi Arabia, 1988. [CrossRef]
26. Al-Mahbashi, A.M.; Elkady, T.Y.; Alrefeai, T.O. Soil water characteristic curve and improvement in lime treated expansive soil. *Geomech. Eng.* **2015**, *8*, 687–706. [CrossRef]
27. Al-Mahbashi, A.M.; Elkady, T.Y. Prediction of unsaturated shear strength of expansive clays. *Geotech. Eng.* **2017**, *170*, 407–420. [CrossRef]
28. Al-Mahbashi, A.M.; Al-Shamrani, M.A.; Abbas, M.F. Hydromechanical behavior of unsaturated expansive clay under repetitive loading. *J. Rock Mech. Geotech. Eng.* **2021**, *13*, 1136–1146. [CrossRef]
29. *ASTM D698-2000*; Standard Test Methods for Laboratory Compaction Characteristics of Soil Using Standard Effort (12400 ft-lbf/ft3 (600 kNm/m^3)). ASTM International: West Conshohocken, PA, USA, 2000; Volume 4.08.
30. *BS EN 13286-53*; Unbound and Hydraulically Bound Mixtures. Methods for the Manufacture of Test Specimens of Hydraulically Boundmixtures Using Axial Compression. British Standard Institute: London, UK, 2004.
31. Blewett, J.; Blewett, I.J.; Woodward, P.K. Phase and Amplitude Responses Associated with the Measurement of Shear-Wave Velocity in Sand by Bender Elements. *Can. Geotech. J.* **2000**, *37*, 1348–1357. [CrossRef]
32. Da Fonseca, A.V.; Ferreira, C.; Fahey, M. A framework interpreting bender element tests, combining time-domain and frequency-domain methods. *Geotech.Test. J.* **2009**, *32*, 91–107.
33. Ogino, T.; Kawaguchi, T.; Yamashita, S.; Kawajiri, S. Measurement Deviations for Shear Wave Velocity of Bender Element Test Using Time Domain, Cross-Correlation, and Frequency Domain Approaches. *Soils Found* **2015**, *55*, 329–342. [CrossRef]
34. Greening, P.D.; Nash, D.F.T. Frequency Domain Determination of G0 Using Bender Elements. *Geotech. Test. J.* **2004**, *27*, 288–294.
35. *ASTM D5856*; Standard Test Method for Measurement of Hydraulic Conductivity of Porous Material Using a Rigid-Wall, Compaction-Mold Permeameter. ASTM International: West Conshohocken, PA, USA, 1995.
36. Vucetic, M.; Dobry, R. Effect of soil plasticity on cyclic response. *J. Geotech. Engrg. Div. ASCE* **1991**, *117*, 89–107. [CrossRef]
37. Lanzo, G.; Vucetic, M. Effect of soil plasticity on damping ratio at small cyclic strains. *Soils Found.* **1999**, *39*, 131–141. [CrossRef]
38. Tatsuoka, F.; Lo Presti, D.C.F.; Kohata, Y. Deformation Characteristics of Soils and Soft Rocks Under Monotonic and Cyclic l-oads and Their Relations. In Proceedings of the 3rd Intemational Conference on Recent Advances in Geotechnical Earthquake Engineerıng and Soil Dynamic, St. Louis, MO, USA, 2–7 April 1995. State of the Art 1(2), 85 I-879.
39. Presti, D.C.L.; Pallara, O.; Cavallaro, A. Damping Ratio of Soils from Laboratory and in Situ Tests. In *Seismic Behaviour of Ground and Geotechnical Structures*; e Pinto, P.S.S., Ed.; CRC Press: Boca Raton, FL, USA, 2021; pp. 391–400.
40. Kumar, S.S.; Krishna, A.M.; Dey, A. Evaluation of dynamic properties of sandy soil at high cyclic strains. *Soil Dyn. Earthq. Eng.* **2017**, *99*, 157–167. [CrossRef]
41. Hussain, M.; Sachan, A. Effect of loading conditions and stress history on cyclic behavior of Kutch soil. *Geomech. Geoengin.* **2020**, *15*, 233–251. [CrossRef]
42. *ASTM D3999/D3999M−11*; Standard Test Methods for the Determination of the Modulus and Damping Properties of Soils Using the Cyclic Triaxial Apparatus. ASTM: West Conshohocken, PA, USA, 2013.
43. Sahaphol, T.; Miura, S. Shear moduli of volcanic soils. *Soil Dyn. Earthq. Eng.* **2005**, *25*, 157–165. [CrossRef]
44. Gratchev, I.B.; Sassa, K.; Osipov, V.I.; Sokolov, V.N. The liquefaction of clayey soils under cyclic loading. *Eng. Geol.* **2006**, *86*, 70–84. [CrossRef]
45. Wang, Y.; Benahmed, N.; Cui, Y.J.; Tang, A.M. A novel method for determining the small-strain shear modulus of soil using the bender elements technique. *Can. Geotech. J.* **2017**, *54*, 280–289. [CrossRef]
46. Albers, B. Linear elastic wave propagation in unsaturated sands, silts, loams and clays. *Transp. Porous Media* **2011**, *86*, 537–557. [CrossRef]

47. Wang, Q.; Cui, Y.J.; Tang, A.M.; Barnichon, J.D.; Saba, S.; Ye, W.M. Hydraulic conductivity and microstructure changes of compacted bentonite/sand mixture during hydration. *Eng. Geol.* **2013**, *164*, 67–76. [CrossRef]
48. Cai, Y.; Yu, Y.; Yuan, X.; Wang, J.; Guo, L. Soil dynamics and geotechnical earthquake engineering. *China Civ. Eng. J.* **2016**, *49*, 9–30.
49. Tao, G.; Kong, L. Permeability coefficient model of saturated/unsaturated soil based on microscopic pore channels and its application. *Shuili Xuebao* **2017**, *48*, 702–709.
50. Gray, D.H.; Rex, R.W. Formation Damage in Sandstones Caused by Clay Dispersion and Migration. *Clays Clay Min.* **1996**, *14*, 355. [CrossRef]
51. Marot, D.; Bendahmane, F.; Rosquoët, F.; Alexis, A. Internal flow effects on isotropic confined sand-clay mixtures. *Soil Sediment Contam.* **2009**, *18*, 294–306. [CrossRef]
52. Sharma, M.M.; Yortsos, Y.C. Fines Migration in Porous Media. *AIChE J.* **1987**, *33*, 1654. [CrossRef]

Disclaimer/Publisher's Note: The statements, opinions and data contained in all publications are solely those of the individual author(s) and contributor(s) and not of MDPI and/or the editor(s). MDPI and/or the editor(s) disclaim responsibility for any injury to people or property resulting from any ideas, methods, instructions or products referred to in the content.